Journal of Alloys and Compounds 789 (2019) 996–1007

Contents lists available at ScienceDirect

Journal of Alloys and Compounds

journal homepage: http://www.elsevier.com/locate/jalcom

Effects of graphene nanosheets on the ceramic coatings formed on Ti6Al4V alloy drill pipe by plasma electrolytic oxidation

Wanying Liu [a, b, d], Carsten Blawert [d], Mikhail L. Zheludkevich [d, e], Yuanhua Lin [a, c, *], Mohd Talha [a], Yunsheng Shi [a], Long Chen [a]

[a] School of Materials Science and Engineering (Southwest Petroleum University), Chengdu, Sichuan 610500, China
[b] School of Materials Science and Engineering (Sichuan University), Chengdu, Sichuan 610065, China
[c] State Key Laboratory of Oil and Gas Reservoir Geology and Exploitation (Southwest Petroleum University), Chengdu, Sichuan 610500, China
[d] Institute of Materials Research, Helmholtz Zentrum Geesthacht, Max-Planck-Str. 1, 21502 Geesthacht, Germany
[e] Faculty of Engineering, University of Kiel, Kaiserstrasse 2, 24143 Kiel, Germany

ARTICLE INFO

Article history:
Received 15 January 2019
Received in revised form
3 March 2019
Accepted 4 March 2019
Available online 5 March 2019

Keywords:
Ceramic coatings
Ti6Al4V alloy
Plasma electrolytic oxidation
Silicate electrolyte
Graphene nanosheets

ABSTRACT

Ceramic coatings were formed on the surface of Ti6Al4V alloy drill pipe by plasma electrolytic oxidation (PEO) technology in the silicate electrolyte with and without graphene nanosheets. Voltage-time responses were recorded. The microstructure, elements distribution and phase composition were investigated by SEM, TEM, EDS and XRD. The basic physical properties and wear resistance were studied. The morphology of wear tracks was observed by SEM and three-dimensional microscope. Results indicated graphene nanosheets successfully incorporated in the ceramic coating. The main elemental components were Ti, Si and O. They were crystallized and composed of anatase and rutile. The coating with graphene nanosheets showing the morphology and structure of flatter and less pores was superior to the coating without graphene nanosheets exhibiting rugged and more pores, and the microhardness of the coating with graphene nanosheets was 1250 HV which was noteworthy improved in contrast with the coating without graphene nanosheets of 870 HV. Wear test results showed the coating with graphene nanosheets displayed extremely significant wear resistance due to the physical barrier of graphene nanosheets. In summary, the application of graphene nanosheets to improve the wear resistance of titanium alloy drill pipe is a promising and promotional research.

1. Introduction

Titanium alloys are widely used as the petroleum drill pipe materials due to the light weight, high strength, good toughness, good corrosion resistance, fatigue resistance and good process performance. However, because of the low hardness and poor wear resistance, it is prone to be worn in the exploration and development drilling of oil and gas field, especially in deep wells, large displacement wells, horizontal wells and high-angle wells. The wear of drill pipe will cause significant damage to the oil and gas field. Plasma electrolytic oxidation (PEO), also referred as micro arc oxidation (MAO), is a novel electrochemical process that involves anodic polarization, thermal oxidation above the dielectric breakdown voltages, which generates short-lived plasma micro discharge at the electrolyte/coating interface. It's a novel and environmental surface treatment technique to produce ceramic coatings with unique and prominent properties on light metal materials such as Mg, Al, Ti and their alloys, and so on [1–4]. In addition to being used in the petroleum drill pipe materials, titanium and titanium alloys are also widely used in other industrial fields, such as aerospace, mechanical, offshore engineering and so on. Unfortunately, the same defect of the poor wear resistance and low hardness also results in the poor toughness, sever adhesive wear and deforming [5–7]. Therefore, that seriously restricts extensive applications of titanium and titanium alloys in various industry sectors. At present, lots of surface treatment methods and technologies have been explored to improve the surface properties of titanium and titanium alloys such as carburizing, coatings and plasma nitriding. However, those methods can only obtain the thin nitrided layer after a long treatment time. The coatings don't have the sufficient durability or the bearing capacity of the load. As one

* Corresponding author. School of Materials Science and Engineering (Southwest Petroleum University), Chengdu, Sichuan 610500, China.
E-mail address: yhlin28@163.com (Y. Lin).

https://doi.org/10.1016/j.jallcom.2019.03.060
0925-8388/

conventional technique, anodic oxidation is the processing for surface oxidation layer of the titanium and titanium alloys. But the ceramic coatings fabricated on titanium alloys by this method are very thin. The thickness is less than one micron [8,9]. So it's rather difficult to improve the properties of titanium and titanium alloys by this surface treatment technique.

Plasma electrolytic oxidation is the unique technique to produce the hard and thick ceramic coatings on titanium and titanium alloys. Essentially, the process of the plasma electrolytic oxidation combing the electrochemical oxidation with a high-voltage spark treatment are adopted [10,11]. The coatings present high hardness, good toughness and adhesion to the substrate due to the in-situ growth of the ceramic coatings. The metallic ions from the matrix material will form when the oxygen ions come out from the electrolyte. The quality and effect of the ceramic coatings can be easily controlled by changing the technique parameters such as the phase composition from the matrix material, the formulation of the electrolyte, and various electrical parameters etc. [12–16]. Xue et al. researched the influence of electrolyte on the microstructure of MAO coatings prepared on Ti-6Al-4V alloy and found that the good morphology, microstructure and performance of ceramic coatings formed in silicate electrolyte could be obtained [17]. Yao et al. studied the preparation and structure of coatings which contains zirconium oxide on the titanium alloy. The results showed that the comprehensive properties of the coatings can be improved due to the zirconium incorporated in the coatings [18]. Li et al. made the analysis of structures and properties about ceramic coatings on TiAl intermetallic compound. It was found that the coatings had the good adhesion and oxidation resistance [12]. However, few systematic researches on the influence of the addition of nanometer particles into the electrolyte on the microstructure, morphology and properties of the ceramic coatings produced by PEO technique are reported.

Therefore, combined with the advantage of plasma electrolytic oxidation technology, the oxidation treatment on the surface of titanium alloy drill pipe are performed using plasma electrolytic oxidation technology in this study, and a new method and idea for surface treatment of petroleum drilling materials are proposed. In the present work, the ceramic coatings were formed on Ti6Al4V titanium alloy by plasma electrolytic oxidation with a direct-current (DC) power supply in the silicate system electrolyte with and without graphene. Voltage-time behaviors were studied and analyzed. The phase constituent and microstructure of the ceramic coatings were analyzed by X-ray diffraction (XRD), scanning electron microscopy (SEM), and transmission electron microscope (TEM). The wear resistance of the uncoated Ti6Al4V alloy and coated samples with and without graphene nanosheets were tested and analyzed. The formation mechanism of the ceramic coatings and the mechanism of wear resistance of the coated samples are also explored in detail.

2. Experimental details

The experimental material is Ti6Al4V titanium alloy (0.06% C, 0.28% Fe, 0.03% N, 0.011% H, 0.15% O, 5.8% Al, 4.1% V, and balance Ti) used as the drill pipe material. It's provided by Tarim oilfield, China. Prior to the plasma electrolytic oxidation process, the original specimens with dimensions of 15 mm × 15 mm × 3 mm were used as substrate material for titanium dioxide coating deposition, and the specimens were ground using emery sheets up to 1200 grit, and then rinsed in ethanol prior to drying in cool air. The ceramic coatings were fabricated on Ti6Al4V titanium alloy using a home-made 20 kW DC power supply. It was mainly composed of DC high-voltage pulsed power supply, electrolytic container, stirring system and water cooling system. The schematic diagram of the device was shown in Fig. 1. Stainless steel plate was acted as the cathode. During the whole process of PEO treatment, the frequency was set to 150 Hz and the oxidation time was selected as 10 min. The Ti6Al4V alloy sample was connected to the anode. The stainless steel plate was used as the counter electrode as well as water cooling system. The constant current density was set as 4 A/dm^2. The duty cycle was 20%. The temperature of electrolyte was controlled below 25 °C. Specimens after finishing PEO treatment were rinsed with distilled water and dried in warm air. The electrolyte was consisted of sodium silicate (5 g/L), sodium phosphate (2 g/L), sodium hydroxide (2 g/L), glycerol (6 ml/L), with and without graphene nanosheets (1 g/L). The ceramic coating produced in the electrolyte without graphene nanosheets was named as G0, and the coating fabricated in the electrolyte with graphene nanosheets was noted as G1. The pH value of two electrolytes (the electrolytes without and with graphene) was tested using a Metrohm 691 pH meter, and they were 12.75, 12.93, respectively. The conductivity of the two electrolytes was measured by a Mettler Toledo Inlab 730 probe. They were 38.86 ms/cm and 48.3 ms/cm, respectively.

The thickness of the PEO coated samples was tested by VT-201 eddy-current thickness gauge. That in three different positions of each coated sample was tested and three samples in each electrolyte were tested. The average value of the thickness was calculated for representing the thickness of PEO coated specimens. The surface microstructure of the ceramic coatings and the microstructure of the polished cross-section mounted in epoxy resin were studied using scanning electron microscopy (SEM, Quanta 450). The element composition of the coatings was tested by the accessorial EDS analysis. All specimens detected by SEM were sputtered with a thin gold layer for preventing the surface charging effects. The X-ray diffraction was performed using DMAX-3A X-ray diffraction (XRD) (Cu Kα radiation, the wave length λ = 1.5406 Å) with the step size of 0.02° and a scan range of 10°–80° to identify the phase constituents of the PEO ceramic coatings. The X-ray generator settings were 45 kV and 40 mA, respectively. The thickness of the ceramic coatings was measured using VT-201 eddy-current thickness gauge, and the thickness of the cross-section coatings was analyzed by SEM. In order to evaluate microstructure and verify graphene successfully incorporated to the PEO coating G1 in detail, transmission electron microscope (TEM, JEL-2100) was used to investigate the cross sectional microstructure of the coating. The microhardness of the coatings was measured by a HX-1 Vickers hardness tester, and the wear test on the coatings and Ti6Al4V alloy

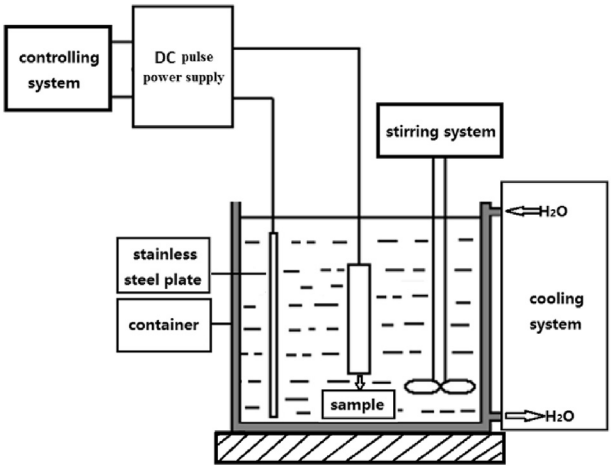

Fig. 1. The schematic diagram of the experimental device.

substrate were carried out on the MFT-4000 multifunctional material surface tester under the dry experiment conditions at the room temperature. The wear test was performed at a normal load of 5 N specimens reciprocated against the steel ball with the maximum linear speed 5 cm/S. For identifying the dominant wear mechanism, the worn surfaces and wear debris were observed and analyzed by SEM, and EDX analysis of the wear track was carried out. Meanwhile, 3D morphologies of the wear tracks of Ti6Al4V alloy substrate, G0 and G1 were also characterized and studied using three-dimensional microscope (ContourGT InMotion GTK-16-0314).

3. Results and discussion

3.1. Voltage-time responses

Voltage-time responses of Ti6Al4V titanium alloy coatings G0 and G1 are presented in Fig. 2. It can be obviously seen that two stages are included in the PEO process. In the first stage, the voltage of two electrolytes linearly increases to nearby 410 V and 340 V in the first 3 min. The average slope of G0 and G1 is 145.5 V/min and 136.3 V/min, respectively. In the PEO process, the obvious white sparks were observed and they were distributed uniformly on the surface of Ti6Al4V alloy substrate, which moved fast and randomly until the voltage reached to 410 V. However, the voltage increases slowly and becomes stable in the second stage. As well-known, the electrical conductivity and melting point of the components which were formed in the anode/electrolyte interface are the two most important factors that significantly affected the voltage of the electrolyte during the PEO treatment [19]. The voltages depend on the electrolyte conductivity, and it decreases with an increase of the electrolyte conductivity [20]. Melting point of the components in the anode/electrolyte interface also affected the voltage. The components with higher melting points possessed higher voltages [21]. The other factor that might affect more or less the voltage was the adsorption of the nano additives at the anode/electrolyte interface [22]. It was also reported that the voltage was affected by the melting point of the oxide components at the anode/electrolyte interface [19]. Therefore, from Fig. 2, it can be easily concluded that the voltage of G0 is higher than that of G1, and the final voltage of G0 and G1 is 452 V, 430 V, respectively. Sarbisheiet al. analyzed the different stages of the Voltage-time during the PEO process, and it was found that the impedance of the coatings slightly increased with the increase of the oxidation voltage and the main process of coating formation is attributed to the constant voltage and monotonous arcs [23]. Based on the study result of Sarbishei et al. [23], the inference that the impedance of the coating G1 is superior to that of the coating G0 can be obtained.

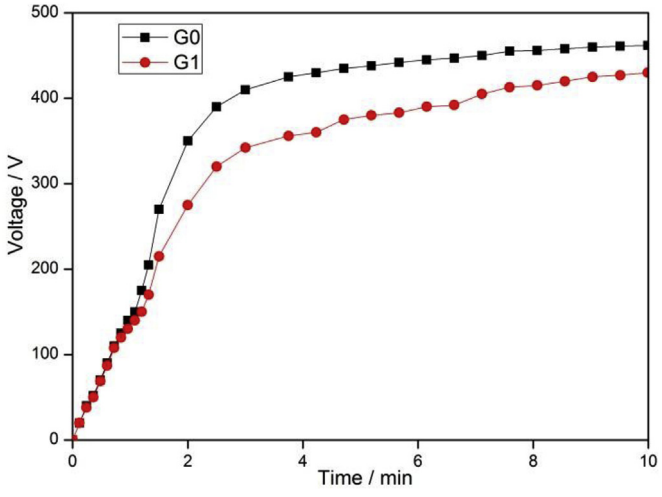

Fig. 2. Voltage-time responses of Ti6Al4V alloy.

3.2. Thickness of the coatings

Table 1 is the thickness value of the ceramic coatings G0 and G1. The thickness of G0 is less in almost all places measured and values are almost uniform for both the coatings as shown in Table 1. Additionally, it can be seen that the thickness of the coating G0 is not uniform from Table 1. The coating in some positions is thick, but it is thin in most area of the coating. The average value of the thickness is 15.7 μm. However, the coating G1 is flat and uniform. The average value of the thickness is 16.1 μm. Graphene has the characteristic of strong interaction among electrons and between electrons and honeycomb grids. Electrons from graphene not only interact strongly with the honeycomb lattice, but also have a strong interaction. That causes the electrons from graphene to interact with the electrons from the electrolyte. They combine tightly each other and form a thick ceramic coating [24–26]. Consequently, the thickness of G1 is higher than that of G0.

3.3. XRD analysis of the coatings

Fig. 3 displayed the X-ray diffraction pattern of PEO ceramic coatings fabricated in different electrolytes. It is clearly found that the coatings are mainly consisted of Ti matrix, rutile TiO_2 and a small amount of anatase TiO_2. The rutile TiO_2 and anatase TiO_2 with the octahedral structure are the allotropes. The bond energy of rutile TiO_2 is larger than that of anatase TiO_2, which belongs to the stable phase. So the physical and chemical properties of the rutile TiO_2 are much more stable than that of the anatase TiO_2. The anatase will transform into rutile when the heating temperature is higher than 700 °C [27]. The increase of the rutile TiO_2 content causes the hardness of coatings to increase and the wear resistance to improve. When the temperature is higher than 700 °C, the anatase starts to transform to the more stable rutile phase. Therefore, the content of anatase TiO_2 in the coatings gradually decreases and the content of the rutile TiO_2 gradually increases with the PEO time prolonging. That will greatly improve the wear resistance of the ceramic coatings.

3.4. Morphology and composition of PEO coatings

Fig. 4 illustrates the cross-sectional microstructure and the surface feature of the ceramic coatings G0 and G1. It can be noted that the difference of the thickness of the coating G0 and G1 is small. The SEM observation result is consistent of the thickness obtained from the test result by VT-201 eddy-current thickness gauge. Although the coating is not flat, the coating G1 is flatter and smoother than that of G0, so it can be found that the thickness in some positions of the ceramic coating surface (as shown by the red

Table 1
Thickness of the ceramic coatings (unit μm).

Number		Sample 1			Sample 2			Sample 3		
		1	2	3	1	2	3	1	2	3
G0	test value	14.1	14.8	15.7	15.2	15.8	15.3	15.1	15.4	20.1
	average	15.7								
G1	testvalue	15.2	15.6	16.2	15.3	15.8	15.5	16.8	18.7	16.2
	average	16.1								

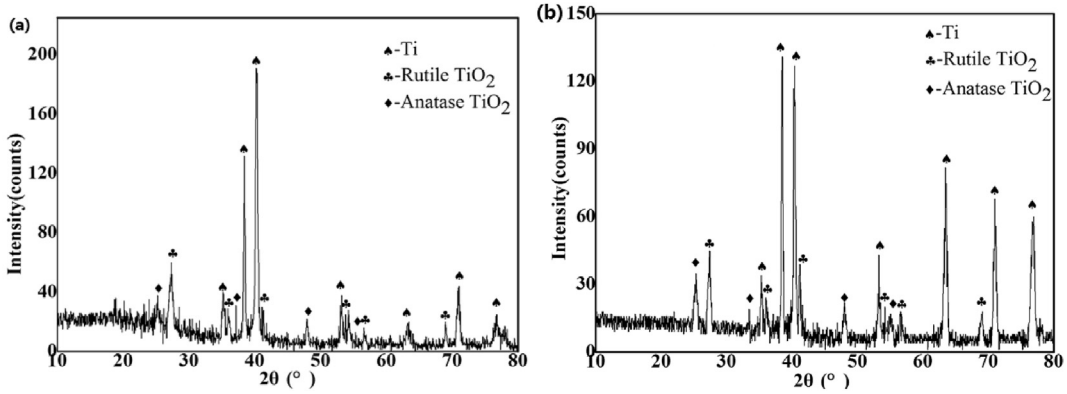

Fig. 3. XRD pattern of PEO coatings formed on Ti6Al4V alloy in the silicate electrolyte: (a) with graphene, and (b) without graphene.

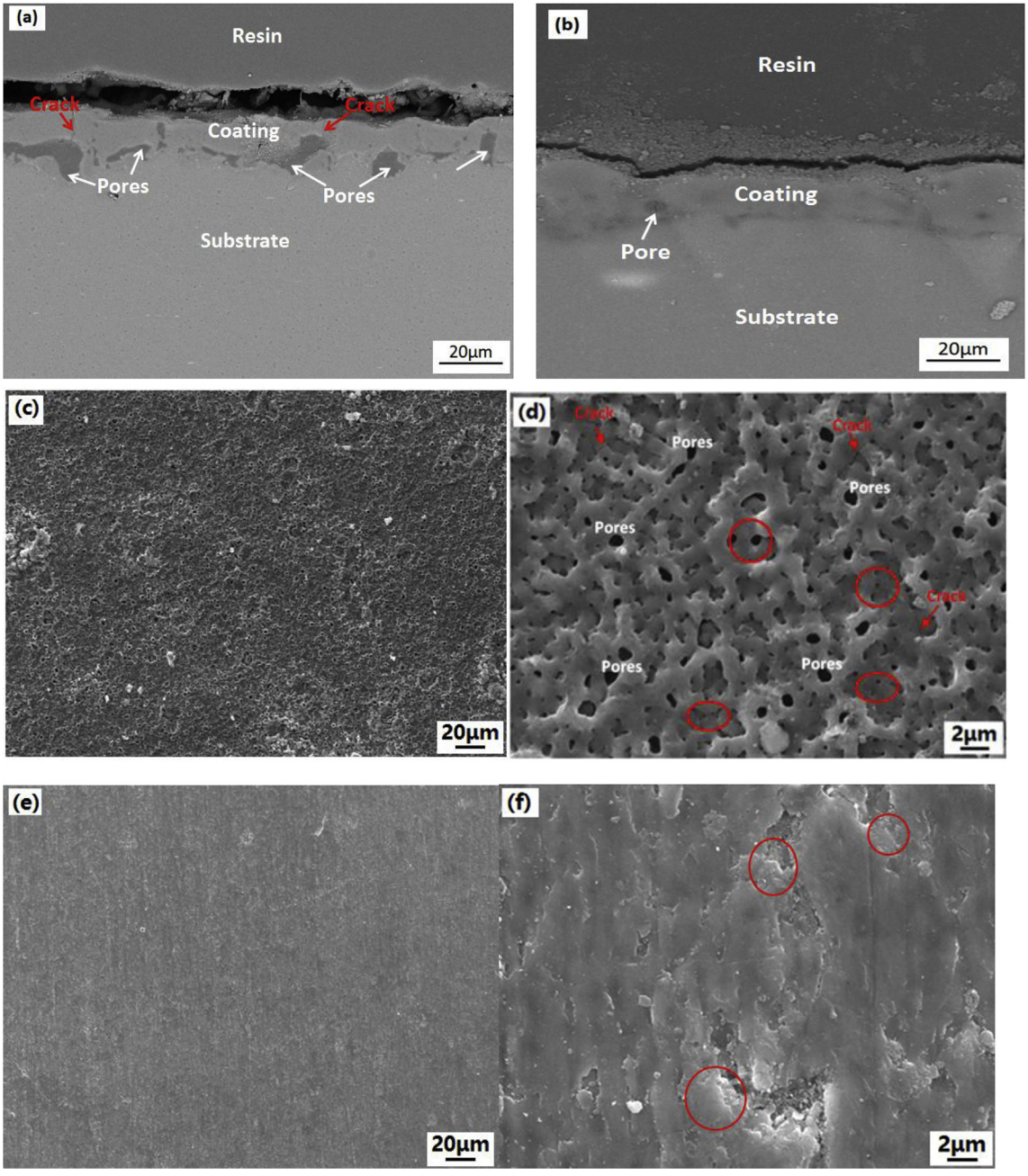

Fig. 4. Section microstructure of the ceramic coatings ((a) and (b)) and surface morphology of the ceramic coatings (from (c) and (f)): (a), (c) and (d): G0; (b), (e) and (f): G1.

circles in Fig. 4(f)) is bigger than that in other positions surface (as shown by the red circles in Fig. 4(d)). Moreover, it can be clearly observed that the surface of the coating in Fig. 4(b) is comparatively flat, dense, and compact than that of the coating in Fig. 4(a). The pores are hardly seen on the surface of the coating G1. Furthermore, the coating is generally uniform, but the coating in Fig. 4(a) is rougher and more uneven. Additionally, some pores exist on it. It can be seen that many micropores with similar sizes and some micro-cracks on the surface of the coating G0 (illustrated in Fig. 4(c) and (d)). The PEO coating G0 exhibits a porous surface in which the micropores with ~1 μm in diameter are uniformly distributed. From the higher magnification it can be clearly seen that the surface of the PEO coating is rough, pores and micro-cracks (Fig. 4 (d)). A greater thermal stress is produced during the process of the PEO treatment, which results in generating numerous of micropores and micro-cracks. However, the coating G1 is flat, smooth and compact (shown in Fig. 4(e) and (f)). Almost no pores distributed on the surface. Only a gully can be found on the surface of the coating. In a word, the morphology of the coating G1 is better than that of G0. It is well known that PEO is the surface treatment technology based on the conventional anodic oxidation of metals and their alloys in various electrolytes. In some degree, it differs from the conventional anodic oxidation by the discharge feature. The spark discharge will generate when the applied voltage exceeds the critical breakdown voltage of the insulated coatings. The coating is not only consisted predominant oxides from the substrate, but also contains complex oxides from the components in the electrolyte [28]. The surface microstructure of the coating G1 is obviously improved in comparison with the coating G0 due to the addition of graphene with strong toughness, lubricity and good conductivity which can fill pores and seal cracks.

The ceramic coatings G0 and G1 were investigated by EDS (sputtered with gold previously). EDS results exhibit the elements distribution in and around the discharged channel. The results are displayed in Fig. 5. EDS detected the common elements silicon, oxygen, titanium, aluminum, vanadium, phosphorus and gold peaks, which arose from the coating incorporated silicon, oxygen, phosphorus from the electrolyte. The element Si is presented in the ceramic coatings. That indicates the SiO_3^{2-} from the electrolyte participates in the reaction of the plasma electrolytic oxidation. The titanium, aluminum and vanadium are arisen from the material matrix. The element Au is the sputtered element previously before EDS test. Based on XRD results that demonstrated that coatings were mainly consisted of Ti matrix, rutile TiO_2 and a small amount of anatase TiO_2, and EDS analysis also demonstrated the presence of Ti, oxygen and Si, the chemical status and the phase composition of the PEO ceramic coatings can be clearly understood by combing the X-ray diffraction analyses with EDS analysis [29,30]. It can be found that XRD result is in agreement with EDS analysis of the coatings and meets their test results. The following is the reactions of PEO processes normally occurring in silicate electrolyte [31–33]:

Conventional anodic processes:

$$Ti \rightarrow Ti^{4+} + 4e^- \quad (1)$$

$$4OH^- \rightarrow O_2\uparrow + 2H_2O + 4e^- \quad (2)$$

Conventional cathodic process:

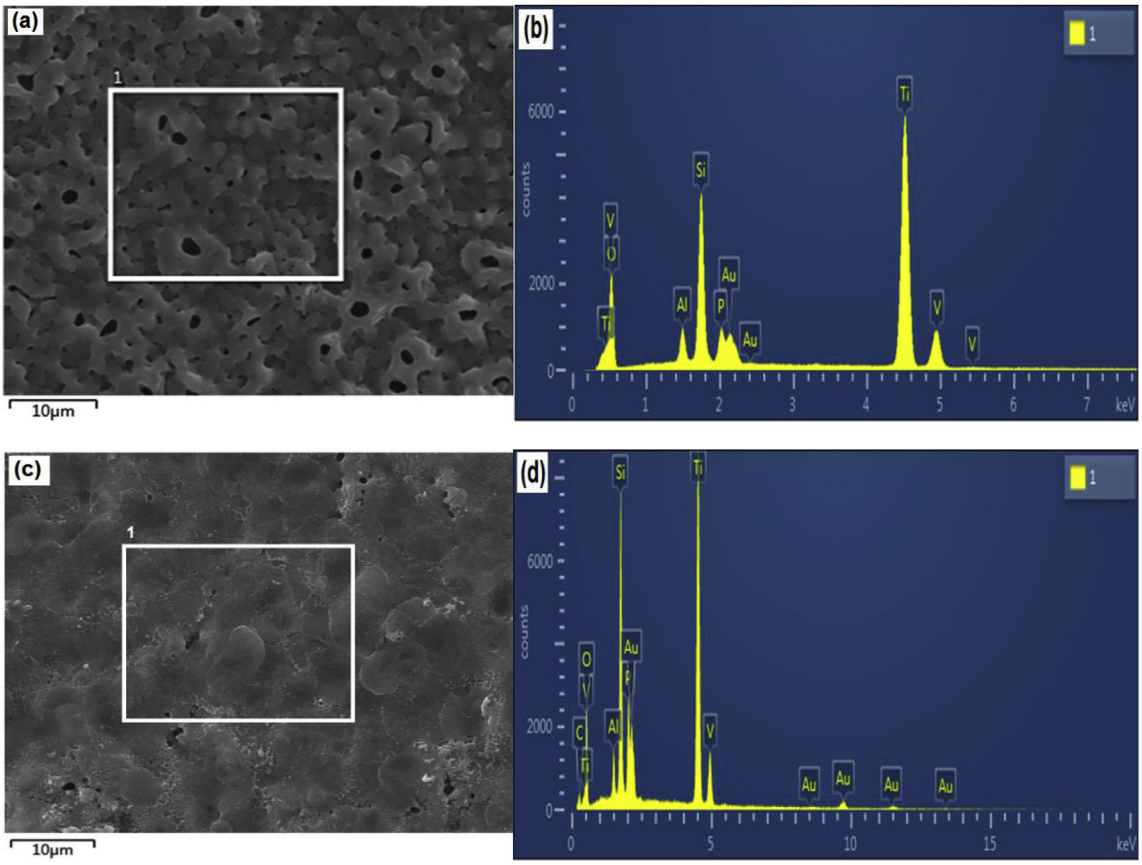

Fig. 5. EDS analysis results on the surface of ceramic coatings G0 and G1: (a), (c) morphology; and (b), (d) EDS spectra.

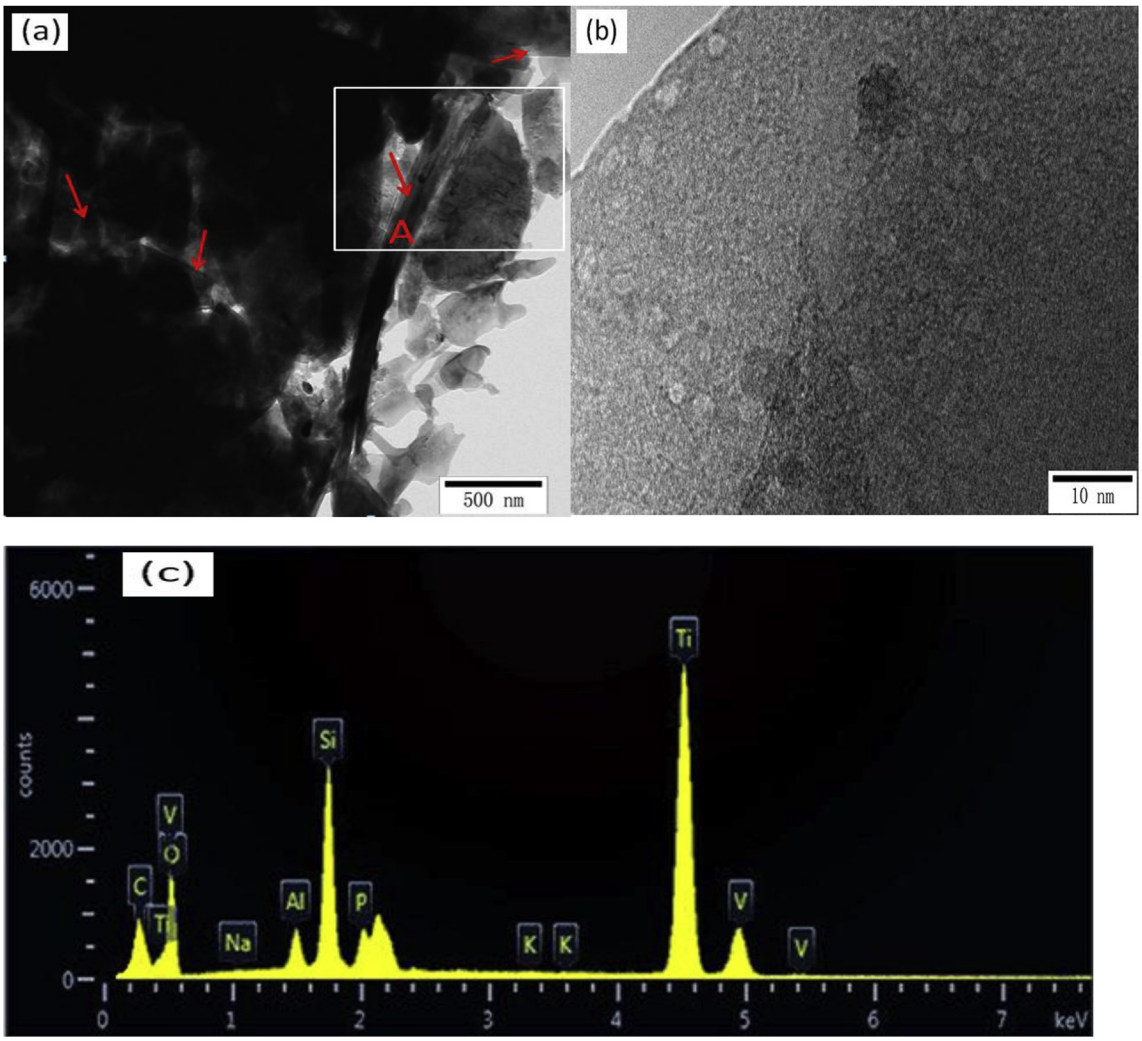

Fig. 6. Cross-sectional TEM images of PEO coatings G1: (a) Brightfield micrograph of oxide layer, (b) HRTEM of graphene embedded in the PEO coating G1 was captured from the rectangular area in (a), (c) EDS spectrum of the selected region.

$$2H_3O^+ + 2e^- \rightarrow H_2\uparrow + 2H_2O \quad (3)$$

High temperature sintering process:

$$Ti^{4+} + 4OH^- \rightarrow TiO_2 + 2H_2O \quad (4)$$

Fig. 6 shows cross-sectional TEM images of the coated sample with graphene, which exhibits the most excellent microstructure and wear resistance in this study. According to TEM observation in Fig. 6(a), it is obviously observed that graphene nanosheets are embedded into the coating in form of filling the micropores and microcracks (as indicated by the red arrows). An HRTEM micrograph of the graphene nanosheets is displayed in Fig. 6(b). It can be clearly noted the sheet and layer structure of graphene nanoadditive. Based on the filling and blocking physic effect of incorporated graphene, the PEO coating with graphene G1 exhibited flatter, denser and compacter structure compared with the coating without graphene G0 (Fig. 4). Some mechanisms have been proposed for the PEO coating formed on aluminum alloy with graphene addition [34,35]. To further confirm that the incorporated substance (noted as A) was graphene, EDS spectroscopy analysis was performed (Fig. 6(c)). The result shows that the carbon content in this area is high. Hence the flaky substance here is graphene nanosheet. It is deduced that the sheets annotated by the red arrows (Fig. 6(a)) are also the incorporated graphene.

3.5. Microhardness of the coatings

According to the standard GOST 9450-76, the microhardness of the PEO ceramic coatings was measured by an HVS-1000B hardness tester at a load of 1.96 N applied to a Vickers indenter. The holding time is 15 s. The test result is shown in Fig. 7. The microhardness of Ti6Al4V alloy matrix is also shown for comparison. It's obvious that the microhardness of the ceramic coatings is much higher than that of the Ti6Al4V alloy substrate, which is attributed to the formation of anatase TiO_2 and rutile TiO_2 on the surface of Ti6Al4V alloy. It's well known that the anatase TiO_2 and rutile TiO_2 can improve the hardness of the ceramic coatings. Because the physical properties of rutile TiO_2 such as hardness, conductivity, and thermal stability are better than that of anatase TiO_2, and the content of the rutile TiO_2 increased in the later of PEO process due to the anatase TiO_2 transforming. Fang et al. [36] and N. Hadi et al. [37] studied the effects of oxidation time on microstructure and properties of PEO coatings, and the results showed that the thickness of the coating increased with the increase of the oxidation time. Ma et al. studied the effects of PEO time on the thickness of the coatings by a model and found the increase of the oxidation time can promote the increase of the thickness of the coating [38]. Therefore, the hardness

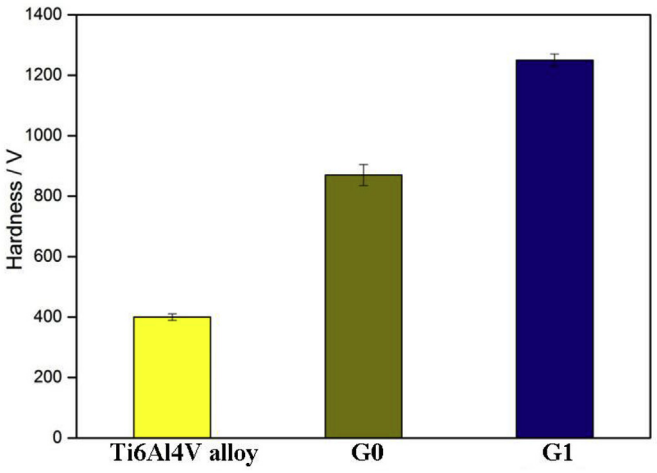

Fig. 7. Microhardness of the ceramic coatings G0, G1 and Ti6Al4V alloy substrate.

of ceramic coatings increased due to the increase of rutile TiO_2 with the extension of the oxidation time. Conclusion that the microhardness of the coating G1 (1250 HV) is higher than that of the coating G0 (870 HV) can be obtained. Additionally, they are both better than the microhardness of Ti6Al4V alloy substrate (400 HV).

3.6. Wear resistance of the coatings

Fig. 8 shows that the friction coefficient of the uncoated Ti6Al4V alloy, the PEO ceramic coatings G0 and G1 under the dry sliding condition with respect to the sliding time. It can be obviously seen that the average friction coefficient of the uncoated Ti6Al4V alloy is 0.78, the average friction coefficient of the ceramic coating G0 and G1 is 0.65, 0.42, respectively. According to some researchers [39–41], the oxide generated in the discharge channel during the PEO process is to favorable decreasing the coating friction. Meanwhile, the rutile TiO_2 and anatase TiO_2 are regarded as a potential low friction coefficient material which can reduce the wear. From Fig. 4, it is clearly observed that the coating G1 is relatively smooth, dense, flat and compact than that of the ceramic coating G0. The ceramic coating G1 has the good morphology and high hardness due to the addition of graphene with the features of good lubricity, high hardness, high strength, good conductivity and so on. That shows the good antifriction properties which are ascribed to the microstructure of the coatings. Furthermore, the ceramic coatings are mainly composed of rutile TiO_2 and anatase TiO_2. TiO_2 specially, the rutile-type is known as a potentially low friction and wear reducing material [42,43].

Wear resistance results are summarized in Fig. 9 which shows the specific wear rate values of the uncoated Ti6Al4V alloy (1.38×10^{-5} mm^3/N.m), G0 (5.06×10^{-6} mm^3/N.m) and G1 (3.62×10^{-6} mm^3/N.m) coated specimens. In this experiment, the wear rate decreased dramatically upon the PEO coatings formed on Ti6Al4V alloy. Especially, G1 exhibited the lowest wear rate among the three samples. The results showed that graphene addition improved the wear resistance of the coating formed on the surface of Ti6Al4V alloy. The tendency of wear rate suggests that the coating G1 displayed better wear resistance due to the effect of incorporated graphene.

The scanning electron micrographs of the wear scars produced on uncoated Ti6Al4V alloy and the coated Ti6Al4V alloy are exhibited in Fig. 10. The wear scar on uncoated Ti6Al4V alloy is much wider than that on PEO coating fabricated in the two electrolytes, which reveals the heavy ploughing because of the adhesive wear (Fig. 10(a and b)). Many plastic deformations occurred on the worn track of uncoated Ti6Al4V alloy surface. However, the wear mechanism of PEO coatings G0 and G1 can be easily obtained according to the scanning electron micrographs of the wear track. The wear mechanism is abrasive wear. The wear resistance of PEO ceramic coatings was obviously improved, and the wear resistance of the coating G1 was better than that of the coating G0 (Fig. 9(c–f)). That can be concluded that the wear resistance of the PEO ceramic coatings lies on its morphology and the phase structure. As is known to all, graphene is the thinnest and hardest nanomaterials in the world, and it has good lubricity [44,45]. Therefore, the ceramic coating with graphene additive significantly improves the wear resistance of Ti6Al4V alloy.

The 3D morphologies of the wear tracks for the uncoated Ti6Al4V titanium alloy, G0 and G1 after the wear tests under a load of 5 N are shown in Fig. 11(a–c), respectively and the wear track depth profiles of the respective specimens are shown in Fig. 11(d). It's obviously observed from Fig. 11 that the wear track of the uncoated Ti6Al4V alloy is very deep after the wear test. However, the PEO coating G0 exhibits shallower wear track than that of the uncoated Ti6Al4V alloy (shown in Fig. 11(b)). The wear track of the PEO coating G1 is very shallow in depth as revealed in Fig. 11(c). The 3D morphologies results are consistent to the SEM morphologies of the worn surface (Fig. 10). The length and width of the wear track of

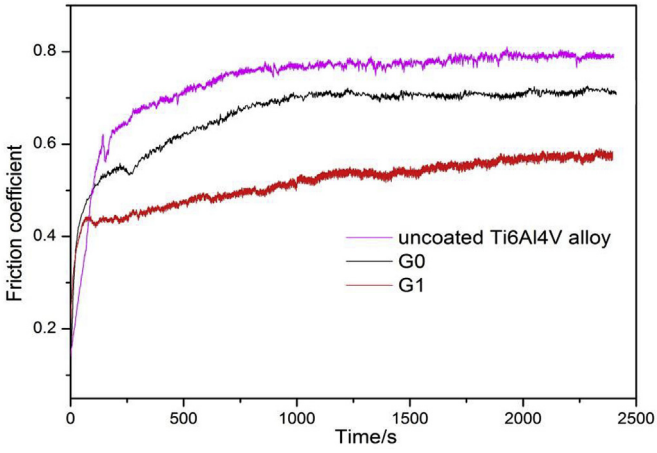

Fig. 8. Friction coefficients of uncoated Ti6Al4V alloy, G0 and G1 with respect to the sliding time.

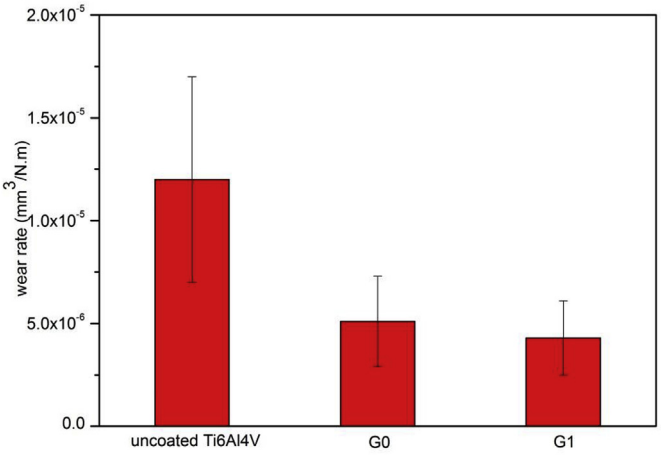

Fig. 9. Specific wear rates of uncoated Ti6Al4V, G0 and G1.

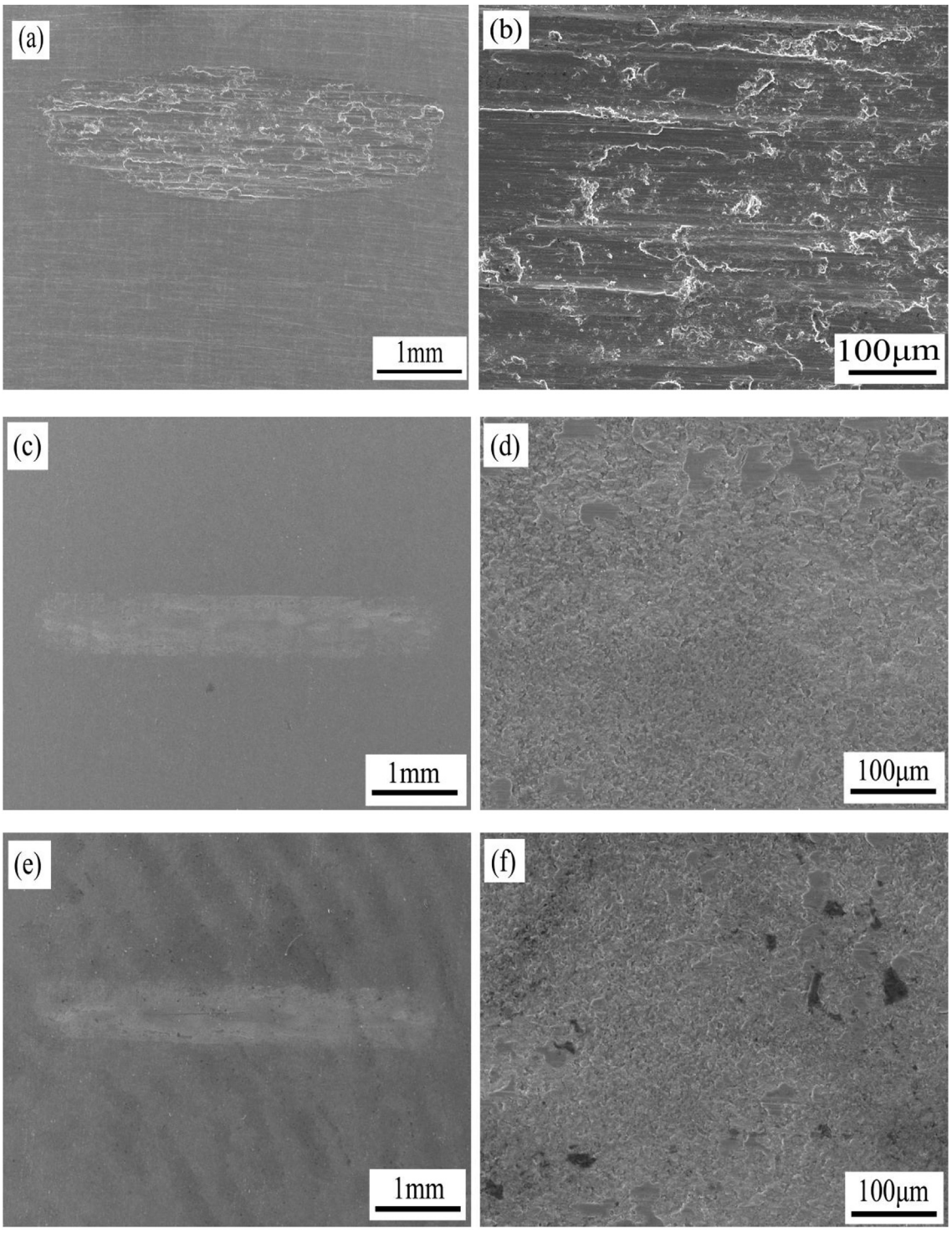

Fig. 10. The wear tracks of the Ti6Al4V alloy substrate (a, b), G0 (c, d), and G1 (e, f).

uncoated Ti6Al4V alloy, G0 and G1 are 5216 ± 1170 μm, 5023 ± 689 μm, and 4328 ± 556 μm, respectively. The above observations were supported by the depth profiles of the wear tracks (Fig. 11(d)). The wear track depth of the uncoated Ti6Al4V alloy, G0 and G1 is found to be around 8.2 μm, 4.1 μm and 1.8 μm, respectively. The test result of the depth of the wear track is agreement with the calculated results of the wear rate of the three samples. According to the definition of the friction coefficient, it's well known that a large friction coefficient will be obtained when the contact area is small. That's to say, the value of the friction coefficient is large at the beginning of wear test. The surface becomes smooth due to the surface protrusion of the object is ground with the increase of the wear. And then the surface roughness gradually reduced, and the wear area increased. Finally the friction coefficient reduced. As the wear increases further, the area of the contact surface tends to be constant, which causes the friction coefficient to be constant. There is a stable stage between the friction stroke and the friction coefficient, and this stage has the largest proportion in

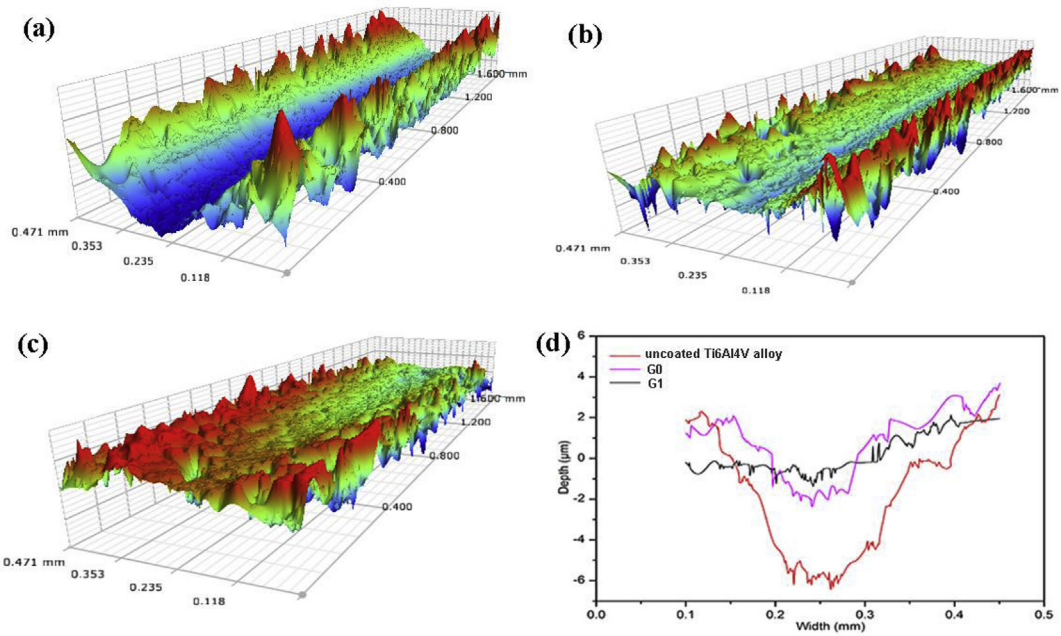

Fig. 11. 3D morphologies of the wear tracks of (a) uncoated Ti6Al4V alloy, (b) G0, (c) G1 and (d) the depth profiles.

the whole process of wear. Until the contact surface is damaged, the actual contact area reduced and the friction coefficient increased [46,47]. Meanwhile, the friction coefficient is only related to the material, and the wear rate is volume of the sample rubbed by the unit friction work. The wear rate is variable. Generally, the larger the friction coefficient is, the greater the wear rate is. Since the surface of the coating G1 is flatter and smoother than that of the coating G0, the friction coefficient of G1 is smaller than that of G0. Then, the wear rate of G1 is smaller than that of G0. The wear amount of G1 is smaller than that of G0. Therefore, the PEO coating with incorporated graphene exhibits excellent tribological property with the lower friction coefficient and wear rate compared to the uncoated Ti6Al4V alloy and the PEO coating without graphene G0, indicating that graphene addition can reduce the friction coefficient and protect the titanium alloy from severe wear. The improvement of the wear resistance is due to the higher hardness of the ceramic coating and the lubricity of incorporation graphene [48,49]. Combined with the SEM morphologies of wear tracks of the three samples, the high wear rate and the deep wear track of the uncoated Ti6Al4V alloy were result from typical features of abrasive and adhesive wear [50].

3.7. Mechanism analysis of PEO coatings formation and wear resistance

The formation mechanism of PEO coatings can be illustrated by Hussein's theory which was denoted as A-, B- and C-type discharges in the PEO processes [51]. A-type discharges happen in the surface holes of PEO coatings, while B-type discharges have penetrated the whole PEO coatings. C-type discharges originate from relatively deep holes of the coatings. A- and C-type discharges are caused by the gas discharges while the B-type discharges derive from the dielectric breakdown in one strong electric field. The B-type discharges, which are caused by the dielectric breakdown, would increase with the increase of applied cathodic voltage [52,53]. At the beginning stage of plasma electrolytic oxidation, a thin insulating coating formed quickly on the surface of specimens by anodic oxidation in the silicate electrolyte. The coating locally occurred crack and broken with the voltage going up to a crucial value (120 V) between the anode and cathode. And then the spark and micro-arc discharges occurred. At this process, the applied voltage exceeded the critical breakdown voltage of the oxide ceramic coating G0 (410 V) and G1 (340 V) on the surface of the metal matrix, the surface passivation film of the metal material matrix would be punctured, and a large number of micro arc discharge zones appeared on the surface of the metal material. The temperature of the electrolyte rapidly rose in the discharging area. That resulted in melting of the weak parts on the surface. The micro-arc discharge channel formed and the complex plasma chemical and electrochemical reaction proceeded in the discharge channel. Consequently, the titanium alloy oxidation products generated. Although the local temperature was very high at the micro-arc discharge moment, the oxidation products with molten state rapidly deposited on the surface of the metal substrate and a ceramic coating formed due to the cooling effect of the electrolyte [54]. Once the high voltage was keeping, numerous sparks would cover the whole surface of the specimen. The previously formed spark and micro-arc spots would quickly move around on the specimen's surface. Both the crater-like surface morphology of coatings and the formation of crystalline TiO_2 such as rutile TiO_2 and anatase TiO_2 with higher melting points confirmed that the temperature in the discharge channels was very high. Therefore, the oxide ceramic coating might be molten locally and temporarily. Nevertheless, the critical cooling rate of forming amorphous TiO_2 phase was very high, but it was very low for SiO_2 of 2×10^{-4} K/s [55]. Therefore, the ceramic coatings mainly contained TiO_2 phase on the surface of Ti6Al4V alloy which consisted of the results in Fig. 3. The rutile TiO_2 and anatase TiO_2 own high hardness and low friction coefficient, so they are considered as the antifriction material. PEO coatings formed on the surface of Ti6Al4V alloy exhibit the good wear resistance, especially, the coating G1 with graphene nanosheets due to its good performances such as high conductivity, high hardness, high elasticity modulus, and high strength.

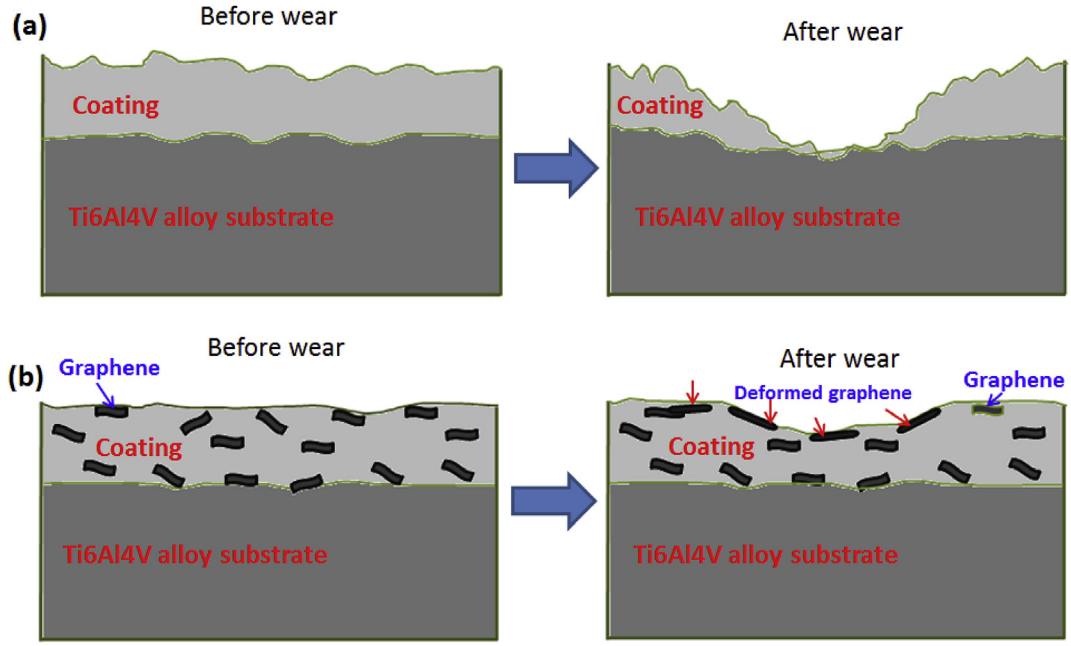

Fig. 12. The formation schematic of the transfer coatings during the wear test.

In order to further explain the mechanism that the coating with graphene addition improves the wear resistance, the changes of the coatings based on the wear test on the surface of the coatings G0 and G1 are illustrated in Fig. 12. It's obviously seen that the depth of wear track is deep and no significant transfer layer could be observed from Fig. 12(a), so the coating exhibited deeper groove under the contact surface in the steel ball back and forth. The mechanism of the wear resistance can be further illustrated according to the references [56–58]. The coating layer is deposited on both sides of the wear track due to the extrusion of the steel ball. The coating in the middle gets thinner and thinner, even the Ti6Al4V substrate was worn too. Furthermore, the coating without graphene shows many microcracks and pores. Hence the positions with microcracks and pores were firstly crack and shed, and then the large area wear appeared. The similar wear mechanism was also elaborated in Ref. [59]. However, for the coating with graphene G1 exhibited a discontinuous deformed graphene layer. The transfer deformed layer reduced the friction coefficient, but could not effectively prevent the removal of the coating away the wear track area from the steel ball rubbing position. That's to say, the worn layer will be deposited away from the interface. Because the coating incorporated graphene, it can successfully fill the microcracks and micropores. Berman et al. [60] also demonstrated that the nano-addition could interfere with the formation of cracks and limited the wear. The coating G1 displayed the denser and compacter microstructure than that of the coating G0, and the hardness was improved significantly. In the process of the wear, graphene occurred deformed and transferred under the wear load, and they were laid flat on the coating in form of barrier layer to block. Additionally, graphene can be used as an additive in conventional lubricants [61]. Kandanur et al. [62] demonstrated that the wear rate of the coating reduced by the incorporated nano-fillers too. So graphene as the nano addition, it can provide a better load-carrying capacity than that of the coating without graphene G0. Therefore, the friction coefficient and wear of the coating G1 decreased due to the addition of graphene nanosheets.

4. Conclusions

(1) A dense ceramic coating of approximately 16 μm can be produced on Ti6Al4V alloy in the silicate electrolyte with and without graphene. The micro-hardness of coated samples (1250 HV and 870 HV) is far greater than that of Ti6Al4V alloy matrix (400 HV). Especially, the maximum microhardness of coated sample with graphene G1 (1250 HV) is higher than that of G0 (870 HV).

(2) Morphological feature of the coated sample G1 is better than that of G2. It shows less pores and micro-cracks, and more smoother, denser, flatter and compacter. Morphological change of the coating during PEO formation includes gradual transformation of original fine grain and the porous structures transformed into a dense fused one.

(3) The ceramic coatings are mainly composed of rutile TiO_2 and anatase TiO_2 according to XRD analysis. PEO coatings significantly improved wear resistance of Ti6Al4V alloy, especially G1 due to the successfully incorporated graphene, that caused the coating thicker, denser, compacter and less pores. So graphene implanted into PEO coatings formed on Ti6Al4V alloy (the wear rate value of G0, G1 of 5.06×10^{-6}, 3.62×10^{-6} mm^3/N.m) effectively improves the wear resistance can be concluded. The novel approach that PEO surface treatment technique combined with addition of graphene nanosheets is applied to improving the wear resistance of Ti6Al4V alloy drill pipe (the wear rate value of 1.38×10^{-5} mm^3/N.m) is a novel and promising approach.

Acknowledgements

The authors wish to thank the funding of the award of fellowship from China Scholarship Council to Wanying Liu, the experiment equipment and technical guidance support by Helmholtz-Zentrum Geesthacht, the financial assistance provided by the National Science Foundation of China (No. 51274170), the 18th college students' key open experimental subjects of Southwest Petroleum

University (No. KSZ18503), and the plan program about passing a test for the young technicist worked in the laboratory (Southwest Petroleum University, 201131010056).

References

[1] G.H. Lv, W.C. Gu, H. Chen, W.R. Feng, M. LatifKhosa, L. Li, E.W. Niu, G.L. Zhang, S.Z. Yang, Characteristic of ceramic coatings on aluminum by plasma electrolytic oxidation in silicate and phosphate electrolyte, Appl. Surf. Sci. 253 (2006) 2947–2952.

[2] F. Liu, F.P. Wang, T. Shimizu, K. Igarashi, L.C. Zhao, formation of hydroxyapatite on Ti–6Al–4V alloy by microarc oxidation and hydrothermal treatment, Suf. Coat. Technol. 199 (2005) 220–224.

[3] G. Sundararajan, L.R. Krishna, Mechanisms underlying the formation of thick alumina coatings through the MAO coating technology, Surf. Coating. Technol. 167 (2003) 269–277.

[4] Y.M. Wang, B.L. Jiang, L.X. Guo, T.Q. Lei, Tribological behavior of microarc oxidation coatings formed on titanium alloys against steel in dry and solid lubrication sliding, Appl. Surf. Sci. 252 (2006) 2989–2998.

[5] Y.M. Wang, B.L. Jiang, T.Q. Lei, L.X. Guo, Microarc oxidation coatings formed on Ti6Al4V in Na2SiO3 system solution: microstructure, mechanical and tribological properties, Surf. Coating. Technol. 201 (2006) 82–89.

[6] K.G. Budinski, Tribological properties of titanium alloys, Wear 151 (1991) 203–217.

[7] A.L. Yerokhin, A. Leyland, A. Matthews, Kinetic aspects of aluminium titanate layer formation on titanium alloys by plasma electrolytic oxidation, Appl. Surf. Sci. 200 (2002) 172–184.

[8] J. Pouilleau, D. Devilliers, F. Garrido, S. Durand-Vidal, E. Mahé, Structure and composition of passive titanium oxide films, Mater. Sci. Eng. B47 (1997) 235–243.

[9] Y. Song, I. Lee, S.N. Hong, B. Kim, K.H. Lee, D.Y. Lee, Corrosion properties of plasma-sprayed Al2O3-TiO2Coatings on Ti metal, J. Mater. Sci. 41 (2006) 2059–2065.

[10] S. Robert, C. Alivait, Ion transport through duplex amorphous/crystalline barrier aluminum oxidation, J. Electrochem. Soc. 135 (1977) 2685–2700.

[11] A.L. Yerokhin, X. Nie, A. Leyland, A. Matthews, Porous Nanocrystalline Titania films by plasma electrolytic oxidation, Suf. Coat. Technol. 154 (2002) 314–318.

[12] X.-J. Li, X.-L. Wu, W.-B. Xue, G.-A. Cheng, R.-T. Zheng, Y.-J. Cheng, Structures and properties of ceramic films on TiAl intermetallic compound fabricated by microarc oxidation, Suf. Coat. Technol. 201 (2007) 5556–5559.

[13] P.I. Butyagin, Y.V. Khokhryakow, A.I. Mamaev, Microplasma systems for creating coatings on aluminium alloys, Mater. Lett. 57 (2003) 1748–1751.

[14] X. Nie, A. Leyland, H.W. Song, A.L. Yerohkin, S.J. Dowey, A. Matthews, Thickness effects on the mechanical properties of micro-arc discharge oxide coatings on aluminium alloys, Surf. Coating. Technol. 116–119 (1999) 1055–1060.

[15] W. Xue, Z. Deng, R. Chen, Z. Zhang, Microstructure and mechanical properties near interface between microarc oxidation coating and Al alloy substrate, Surf. Eng. 16 (2000) 344–352.

[16] A.A. Voevodin, A.L. Yerokh, V.V. Lyubimov, M.S. Doonley, J.S. Zabinski, Characterization of wear protective AlSiO coatings formed on Al-based alloys by micro-arc discharge treatment, Surf. Coating. Technol. 86–87 (1996) 516–521.

[17] W.B. Xue, C. Wang, Z.W. Deng, R.Y. Chen, T.H. Zhang, Influence of electrolytes on the microarc oxidation coatings on Ti-6Al-4V alloy, J. Mater. Sci. Technol. 18 (2002) 37–39.

[18] Z.P. Yao, Y.L. Jiang, Z.H. Jiang, F.P. Wang, Z.D. Wu, Preparation and structure of ceramic coatings containing zirconium oxide on Ti alloy by plasma electrolytic oxidation, J. Mater. Process. Technol. 205 (2008) 303–307.

[19] M. Tang, Z. Feng, G. Li, Z. Zhang, R. Zhang, High-corrosion resistance of the microarc oxidation coatings on magnesium alloy obtained in potassium fluotitanate electrolytes, Surf. Coating. Technol. 264 (2015) 105–113.

[20] S. Ikonopisov, Theory of electrical breakdown during formation of barrier anodic films, Electrochim. Acta 22 (1977) 1077–1082.

[21] M. Laleh, A. SabourRouhaghdam, T. Shahrabi, A. Shanghi, Effect of alumina sol addition to micro-arc oxidation electrolyte on the properties of MAO coatings formed on magnesium alloy AZ91D, J. Alloys Compd. 496 (2010) 548–552.

[22] S. Fatimah, M.P. Kamil, J.H. Kwon, M. Kaseem, Y.G. Ko, Dual incorporation of SiO_2 and ZrO_2 nanoparticles into the oxide layer on 6061 Al alloy via plasma electrolytic oxidation: coating structure and corrosion properties, J. Alloys Compd. 707 (2017) 358–364.

[23] S. Sarbishei, M.A.F. Sani, M.R. Mohammadi, Study plasma electrolytic oxidation process and characterization of coatings formed in an alumina nanoparticle suspension, Vacuum 108 (2014) 12–19.

[24] F. Awaja, M. Tripathi, T.-T. Wong, T. O'Brien, G. Speranza, The chemistry and topography of stabilized and functionalized graphene oxide coatings, Plasma Process. Polym. 15 (2018), e1800084. https://doi.org.10.1002/ppap.201800084.

[25] Y.X. Zhu, C.Y. Duna, H.Y. Liu, Y.F. Chen, Y. Wang, Graphene coating for anticorrosion and the investigation of failure mechanism, J. Phys. D Appl. Phys. (2017) 50.

[26] D.G. Papageorgiou, I.A. Kinloch, R.J. Young, Mechanical properties of graphene and graphene-based nanocomposites, Prog. Mater. Sci. 90 (2017) 75–127.

[27] D.Q. Wei, Y. Zhou, C.H. Yang, Characteristic, cell response and apatiteinduction ability of microarc oxidized TiO_2-based coating containing P on Ti6Al4V before and after chemical-treatment and dehydration, Ceram. Int. 35 (2009) 2545–2554.

[28] C. Fei, Z. Hai, C. Chen, Y.J. Xia, Study on the tribological performance of ceramic coatings on titanium alloy surfaces obtained through microarc oxidation, Prog. Org. Coating 64 (2009) 264–267.

[29] Y. Han, S.H. Hong, K.W. Xu, Porous nanocrystalline titania films by plasma electrolytic oxidation, Surf. Coating. Technol. 154 (2002) 314–318.

[30] M. Khorasanian, A. Dehghan, M.H. Shariat, M.E. Bahrololoom, S. Javadpour, Microstructure and wear resistance of oxide coatings on Ti–6Al–4V produced by plasma electrolytic oxidation in an inexpensive electrolyte, Surf. Coating. Technol. 206 (2011) 1495–1502.

[31] M. Shokouhfar, C. Dehghanian, M. Montazeri, A. Baradaran, Preparation of ceramic coating on Ti substrate by plasma electrolytic oxidation in different electrolytes and evaluation of its corrosion resistance: Part II, Appl. Surf. Sci. 258 (2012) 2416–2423.

[32] G. Lv, H. Chen, L. Li, E. Niu, H. Pang, B. Zou, S. Yang, Investigation of plasma electrolytic oxidation process on AZ91 D magnesium alloy, Curr. Appl. Phys. 9 (2009) 126–130.

[33] R.C. Barik, J.A. Wharton, R.J.K. Wood, K.R. Stokes, R.L. Jones, Corrosion and erosion-corrosion performance of plasma electrolytic oxidation (PEO) deposited Al_2O_3Coatings, Surf. Coating. Technol. 199 (2005) 158–167.

[34] W. Liu, Y. Liu, Y. Lin, Z. Zhang, S. Feng, T. Mohd, Y. Shi, T. Shi, Effects of graphene on structure and corrosion resistance of plasma electrolytic oxidation coatings formed on D16T Al alloy, Appl. Surf. Sci. (2018). https://doi.org/10.1016/j.apsusc.2018.12.233.

[35] R. Pérez-Bustamante, D. Bolaños-Morales, J. Bonilla-Martínez, I. Estrada-Guel, R. Martínez-Sánchez, Microstructural and hardness behavior of graphene-nanoplatelets/aluminum composites synthesized by mechanical alloying, J. Alloys Compd. 615 (2014) S578–S582.

[36] L. Fang, Y.Z. Ma, W.S. Liu, Y. Liu, C. Liu, H.Y. Yan, Effects of oxidation time on microstructure and corrosion resistance of micro-arc oxidation film on aluminum alloy, Mater. Sci. Eng. Powder Metallargy 23 (2018) 503–510 (China).

[37] N. Hadi, E. Reza, A. MasoudKasiri, Tribological performance of PEO-WC nanocomposite coating on Mg alloys deposited by plasma electrolytic oxidation, Tribol. Int. 98 (2016) 253–260.

[38] X. Ma, C. Blawert, D. Hoeche, A model describing the growth of a PEO coating on AM50 Mg alloy under constant voltage mode, Electrochim. Acta 251 (2017) 461–474.

[39] M.P. Kamil, M. Kaseem, Y.G. Ko, Soft plasma electrolysis with complex ions for optimizing electrochemical performance, Sci. Rep. 7 (2017) 44458, https://doi.org/10.1038/srep44458.

[40] G. Wang, X.Y. Nie, J.M. Tjong, Investigation into mixed and hydrodynamic frictions of PEO coatings and cast iron, SAE Int. J. Fuels Lubr. 9 (2016) 23–31.

[41] B. Yin, Z.J. Peng, J. Liang, K.J. Jin, S.Y. Zhu, J. Yang, Z.H. Qiao, Tribological behavior and mechanism of self-lubricating wear-resistant composite coatings fabricated by one-step plasma electrolytic oxidation, Tribol. Int. 97 (2016) 97–107.

[42] Y.M. Wang, B.L. Jiang, T.Q. Lei, Microarc oxidation coatings formed on Ti6Al4V in Na_2SiO_3 system solution: microstructure, mechanical and tribological properties, Surf. Coating. Technol. 210 (2006) 82–89.

[43] Y.M. Wang, B.L. Jiang, T.Q. Lei, Fretting wear behaviour of microarc oxidation coatings formed on titanium alloy against steel in unlubrication and oil lubrication, Appl. Surf. Sci. 252 (2006) 8113–8120.

[44] J.-M. Zhao, X. Xie, C. Zhang, Effect of the graphene oxide additive on the corrosion resistance of plasma electrolytic oxidation coating of the AZ31 magnesium alloy, Corros. Sci. 114 (2017) 146–155.

[45] S. Durdu, M. Usta, The tribological properties of bioceramic coatings produced on Ti6Al4V alloy by plasma electrolytic oxidation, Ceram. Int. 40 (2014) 3627–3635.

[46] G. Sun, H. Zhu, C. Ding, Y. Zhou, Multifractal detrended fluctuation analysis on friction coefficient during the friction process, J. Tribol. Trans. ASME 140 (2018).

[47] M. Alajmi, A. Shalwan, Correlation between mechanical properties with specific wear rate and the coefficient of friction of graphite/epoxy composites, Materials 7 (2015) 4162–4175.

[48] L. Cescaller, E. Lanoni, C. Martini, D. Prandstraller, G. Sambogna, Wear 264 (2008) 86–95.

[49] P. Hvizdoš, J. Dusza, C. Balázsi, Tribological properties of Si_3N_4–graphene nano composites, J. Eur. Ceram. Soc. 33 (2013) 2359–2364.

[50] C.Y.H. Lim, S.C. Lim, M. Gupta, Wear behaviour of SiCp-reinforced magnesium matrix composites, Wear 255 (2003) 629–637.

[51] R.O. Hussein, X. Nie, D.O. Northwood, A. Yerokhin, A. Matthews, Spectroscopic study of electrolytic plasma and discharging behaviour during the plasma electrolytic oxidation (PEO) process, J. Phys. D Appl. Phys. 43 (2010) 1–13.

[52] K. Yang, B. Cao, Electrical characteristics identification of dielectric film breakdown during plasma electrolytic oxidation process, Mater. Lett. 143 (2015) 177–180.

[53] A. Nominé, J. Martin, G. Henrion, T. Belmonte, Effect of cathodic microdischarges on oxide growth during plasma electrolytic oxidation (PEO), Surf. Coating. Technol. 269 (2015) 131–137.

[54] R.K. Prasd, R.G.D. Janaki, B.E. Stucker, Improvement in corrosion resistance of friction stir welded aluminum alloys with microarc oxidation coatings, Scipta

Mater. 58 (2008) 998–1001.
[55] H. Habazakia, S. Tsunekawa, E. Tsuji, T. Nakayama, Formation and characterization of wear-resistant PEO coatings formed on β-titanium alloy at different electrolyte temperatures, Appl. Surf. Sci. 259 (2012) 711–718.
[56] X.S. Li, L.S. He, Y. Yang, Forming mechanism of composite coating with nanoparticles and its wear resistance, Appl. Mech. Mater. 281 (2013) 500–504.
[57] M. Atapour, C. Blawert, M.L. Zheludkevich, The wear characteristics of CeO2 containing nanocomposite coating made by aluminate-based PEO on AM 50 magnesium alloy, Surf. Coating. Technol. 357 (2019) 626–637.
[58] X. Lu, C. Blawert, Y. Huang, H. Ovri, M.L. Zheludkevich, K.U. Kainer, Plasma electrolytic oxidation coatings on Mg alloy with addition of SiO_2 particles, Electrochim. Acta 187 (2016) 20–33.
[59] H. Li, Y. Lei, K. Li, L. Huang, S. Huang, B. Zhao, X. Zheng, Microstructure and wear behavior of graphene nanosheets-reinforced zirconia coating, Ceram. Int. 40 (2014) 12821–12829.
[60] D. Berman, A. Erdemir, A.V. Sumant, Graphene: a new emerging lubricant, Mater. Today 17 (2014) 31–42.
[61] J. Lin, L. Wang, G. Chen, Modification of graphene platelets and their tribological properties as lubricating additive, Tribol. Lett. 41 (2011) 209–215.
[62] S.S. Kandanur, M.A. Rafiee, F. Yavari, M. Schrameyer, Z.Z. Yu, T.A. Blanchet, N. Koratkar, Suppression of wear in graphene polymer composites, Carbon 50 (2012) 3178–3183.